

AAS 16-486



**APPROPRIATE FIDELITY ELECTROSTATIC
FORCE EVALUATION CONSIDERING A RANGE
OF SPACECRAFT SEPARATIONS**

Joseph Hughes and Hanspeter Schaub

**AAS/AIAA Spaceflight Mechanics
Conference**

Napa Valley, California

February 14–18, 2016

AAS Publications Office, P.O. Box 28130, San Diego, CA 92198

APPROPRIATE FIDELITY ELECTROSTATIC FORCE EVALUATION CONSIDERING A RANGE OF SPACECRAFT SEPARATIONS

Joseph Hughes* and Hanspeter Schaub†

Charged spacecraft experience electrostatic forces and torques from both charged neighboring spacecraft and the local space environment itself. The Multi Sphere Method (MSM) is a recent methodology to numerically approximate electrostatic forces significantly faster than realtime. This allows the simulation of the complex charged astrodynamics that can occur with Coulomb tugging and detumbling operations, as well as predicting the charged debris dynamics. This paper develops reduced order electrostatic force models suitable for locally flat electric fields (large separations) and radial fields (medium separation larger than 5-10 craft radii). Unlike MSM, this reduced order expansion derives the force and torque from a first-principles manner, and has no tuning parameters. This adds analytical insight but can sacrifice accuracy in contrast with MSM by removing the tuning parameters.

INTRODUCTION

In the Geosynchronous Earth Orbit (GEO) regime satellites can charge to very high voltages (such as 10s of kilo-Volts in the Earth's shadow).¹ The interactions of this charge with Earth's magnetic field cause significant translational and rotational perturbations of uncontrolled debris, especially High Area to Mass Ratio (HAMR) objects.² A 2 m diameter spacecraft in a LEO orbit charged to 10 kV experiences force of about 2 μ -Newtons in strength, a perturbation that compares with SRP, drag at 500 km, and Lunar gravity.³ Predicting these forces and torques accurately is essential for high-fidelity tracking applications such as Space Situational Awareness (SSA). Spacecraft can also take advantage of these electrostatic forces and torques by controlling their own voltage or that of a neighboring spacecraft, with electron and ion emission.⁴ Strong forces and torques can be applied between charged spacecraft which enable many novel touchless actuation concepts such as the Electrostatic Tractor (ET).⁵⁻⁷

With the ET concept a tug or servicer satellite irradiates a passive deputy spacecraft with an electron beam such that the tug becomes positively charged and the deputy becomes negatively charged. An attractive Coulomb force results from this charging. For two moderately sized spacecraft (3m diameter) charged at ± 20 kV, and separated by 7 craft radii, the deputy feels a 1.2 mN force that could raise its orbit by more than 5 km/day.⁸ A tug craft equipped with an electron gun and low thrust motors could move defunct GEO satellites to a graveyard orbit in a matter of months⁸ where they would no longer pose a collision threat in a very valuable but threatened orbital region.^{9,10} Spacecraft with non-symmetric charge distributions will also feel and apply torques through this

*Graduate Research Assistant, Aerospace Engineering Sciences, University of Colorado.

† Alfred T. and Betty E. Look Professor of Engineering, Associate Chair of Graduate Affairs, Department of Aerospace Engineering Sciences, University of Colorado, 431 UCB, Colorado Center for Astrodynamics Research, Boulder, CO 80309-0431. AAS Fellow

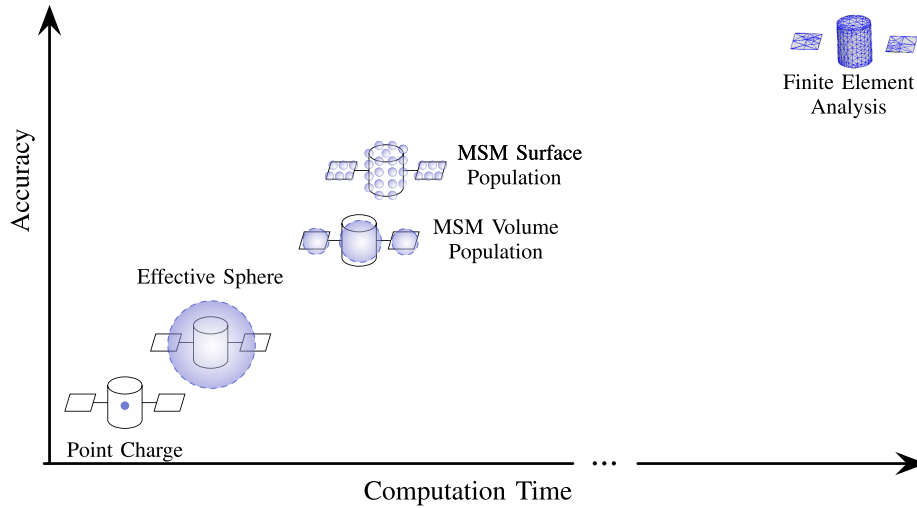


Figure 1. Illustration of computation effort and accuracy for a variety of force and torque models²¹

charging.¹¹ This torque can be used to touchlessly detumble non-cooperative space objects in a matter of days.¹² The ET allows a single mother craft equipped with attitude and position control devices to apply forces and torques to an entire constellation of spacecraft.¹³ Furthermore, if only relative control is required, formation shape control can potentially be achieved with no fuel expenditure.^{14, 15}

One technology that makes use of environmental effects is the electrostatic sail.¹⁶ The sail consists of a web of charged wires that deflect protons in the solar wind and absorb their momentum. With very large tethers at high voltage, this can provide a sustained 0.5 Newtons. Another concept uses the Lorentz force ($\mathbf{F} = q\mathbf{v} \times \mathbf{B}$) to augment an orbit.¹⁷ Augmented LEO orbits,¹⁸ formation flying constellations¹⁹ and assisted gravity assists²⁰ are all attractive options.

Fast and accurate models of torque and force are needed in all of the above applications to prescribe needed Voltages. The electrostatic force and torque can be computed using a range of methods as illustrated in Figure 1. The point charge method is the fastest, but does not take into account any geometry or capacitance relations of the space object. The finite element method is the most precise method but such solutions take a long time to compute. The single-to multi-sphere methods illustrated in the middle sacrifice numerical accuracy for computational efficiency. MSM solutions that are within a few percent can run 1000's to 100,000's times faster than the finite element solution,^{21, 22} depending on the number of spheres used. However, given a specific MSM sphere representation across a conducting space object, the charge evaluation requires a capacitance matrix inverse whose computational efforts scales with N^3 , where N is the number of MSM spheres. Further, to evaluate the force, the inter-sphere forces must be summed up across all spheres. This leads to a somewhat increased computation effort, and yields an analytical MSM solution that is not insightful for analytical charged astrodynamics analysis.

Rather, this paper investigates modified methods to evaluate the electrostatic forces and torques using Appropriate Fidelity Measures (AFMs). The locally flat ($\nabla \mathbf{E} = \nabla \mathbf{B} = 0$) electric and magnetic field environment scenario is a good approximation of an isolated charged space object. Next, a radial electric field is assumed to act on a general conducting body. This scenario applies to

two charged spacecraft that are far enough apart that the complex body geometry can be neglected. To find a fast solution, a truncated Taylor series expansion in the ratio of spacecraft effective radius to separation is used. This scenario is similar to how constant-mass gravity fields of non-symmetric bodies such as asteroids can be approximated through a first order expansion. The results obtained using these truncated Taylor series for force and torque are compared against the FEA truth model in the special case of a cylinder and sphere. Finally, the dynamics of this alternate model are used to predict how the charge distribution and therefore the force and torque will change over time.

MSM OVERVIEW

Commercial electrostatic field solvers such as ANSYS's Maxwell 3D allow for very high fidelity computation of charge distribution, force, and torque. However, this process is much slower than realtime. Propagating three GEO orbits (72 hours of real time) for a simple charged shape using a 10 second timestep with an 4th order Runge-Kutta integration method would take 72 days to complete. The factor of 24 slowdown makes commercial FEA an infeasible option for predicting electrostatic forces and torques.

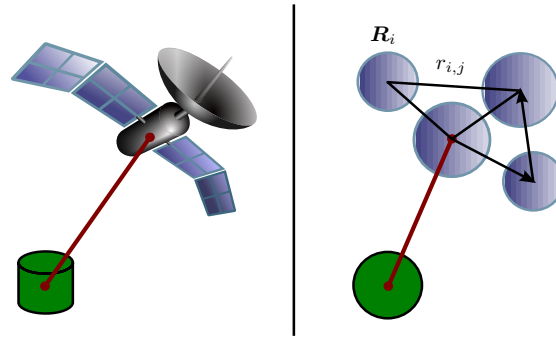


Figure 2. The Multi Sphere Method (MSM) approximates the spacecraft body as a collection of charged spheres²¹

MSM emerged as a way to predict the force and torque with high-enough fidelity to be useful, while also evaluating fast enough to be practical. MSM approximates the satellite as a collection of spheres with variable position and radii. The voltage of any sphere is a function of both it's own charge and the charge on neighboring spheres. If these spheres are far enough away to be approximated as point charges, the Voltage on the i^{th} sphere is given by:²¹⁻²³

$$V_i = \frac{1}{4\pi\epsilon_0} \frac{q_i}{R_i} + \sum_{j=1, j \neq i}^N \frac{1}{4\pi\epsilon_0} \frac{q_j}{r_{i,j}} \quad (1)$$

Where q_i and R_i are the charge and radius of the i^{th} sphere, respectively, and $r_{i,j}$ is the distance between spheres i and j . If the Voltages of each sphere are given by $\mathbf{V} = [V_1, V_2, \dots, V_N]^T$ and the charges are given by $\mathbf{q} = [q_1, q_2, \dots, q_N]^T$, the relationship between the two is $\mathbf{V} = [\mathbf{C}]^{-1}\mathbf{q}$. Where

$[C]$ is the position dependent capacitance (PDC) matrix whose inverse is defined below:

$$[C]^{-1} = \frac{1}{4\pi\epsilon_0} \begin{bmatrix} 1/R_1 & 1/r_{1,2} & \cdots & 1/r_{1,N} \\ 1/r_{2,1} & 1/R_2 & \cdots & r_{2,N} \\ \vdots & \vdots & \ddots & \vdots \\ 1/r_{N,1} & 1/r_{N,2} & \cdots & 1/R_N \end{bmatrix} \quad (2)$$

Since the Voltage is assumed known, and to be uniform across the spacecraft and the charges are needed to compute forces and torques, this matrix can be inverted and solved for the charge on each sphere. Once the charges are known the forces and torques can be computed as shown in Eqns. (3) and (4). We assume an origin at the center of mass of the body for \mathbf{r}_i and allow \mathbf{E} and \mathbf{B} to vary within the body and indicate the velocity of each sphere with respect to the magnetic field as \mathbf{v}_i .

$$\mathbf{F} = \sum_{i=1}^N (\mathbf{E}(\mathbf{r}_i) + \mathbf{v}_i \times \mathbf{B}(\mathbf{r}_i)) q_i \quad (3)$$

$$\mathbf{L} = \sum_{i=1}^N \mathbf{r}_i \times (\mathbf{E}(\mathbf{r}_i) + \mathbf{v}_i \times \mathbf{B}(\mathbf{r}_i)) q_i \quad (4)$$

MSM is an accurate and fast way to solve for the forces and torque on a spacecraft. However, it relies on knowledge of the position and size of all spheres in the model, often laboriously hand tuned. Furthermore, little analytical insight is gained by solving for the forces by inverting the $[C]^{-1}$ matrix in Eq.(2). This paper seeks to find a more elegant way to describe the charge distribution tailored for specific field configurations. Furthermore, the dynamics of this charge distribution subject to an external field are found. This provides analytical insight to the problem of controllability while de-spinning.

ELECTROSTATIC FORCE AND TORQUE DERIVATIONS

The differential force on a differential charge moving at \mathbf{v} subject to \mathbf{E} and \mathbf{B} fields is given by:²³

$$d\mathbf{F} = dq(\mathbf{E} + \mathbf{v} \times \mathbf{B}) \quad (5)$$

Where \mathbf{v} is the velocity of the differential charge with respect to the magnetic field. The torque about the center of mass on a body is defined as $\int_B \mathbf{r} \times d\mathbf{F}$, where \mathbf{r} points from the center of mass to the volume element. Using the differential force to find the force and torque on a body gives:

$$\mathbf{F} = \int_B (\mathbf{E} + \mathbf{v} \times \mathbf{B}) \rho dV \quad (6)$$

$$\mathbf{L} = \int_B \mathbf{r} \times (\mathbf{E} + \mathbf{v} \times \mathbf{B}) \rho dV \quad (7)$$

Where ρ is the charge density (Coulombs/m³) and $\int_B dV$ indicates a volume integral over the spacecraft body. The velocity in the above equations must be taken with respect to the magnetic field. Expressing the velocity in an ECEF frame would be very close to the spacecraft velocity with respect to the magnetic field.

Flat Fields Approximation

If the fields do not change over the spacecraft body as shown in Figure 3, the terms \mathbf{E} and \mathbf{B} can be taken outside the integrals in Eqns. (6) and (7).

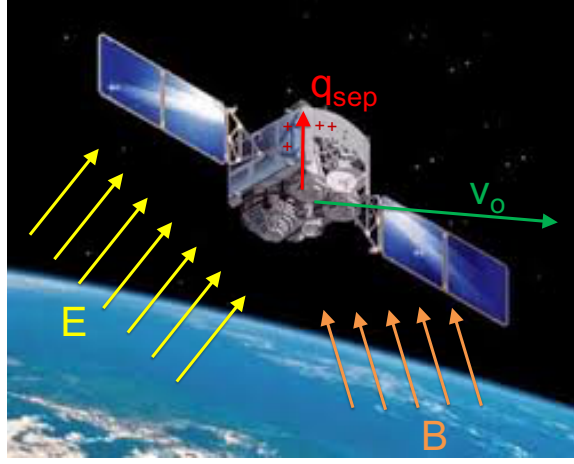


Figure 3. Flat E and B Field Configuration

Force Derivation: To calculate the force experienced by a spacecraft in a flat field, the velocity variation over the body must be accounted for. The velocity is the orbital velocity \mathbf{v}_o plus the transport velocity: $\boldsymbol{\omega}_{\mathcal{B}/\mathcal{E}} \times \mathbf{r}$,²⁴ where $\boldsymbol{\omega}_{\mathcal{B}/\mathcal{E}}$ is the angular velocity between the satellite body frame \mathcal{B} and the magnetic field frame \mathcal{E} . Letting $\mathbf{v} = \mathbf{v}_o + \boldsymbol{\omega}_{\mathcal{B}/\mathcal{E}} \times \mathbf{r}$ in Eq. (6):

$$\mathbf{F} = \mathbf{E} \int_B \rho dV + \int_B (\mathbf{v}_o + \boldsymbol{\omega}_{\mathcal{B}/\mathcal{E}} \times \mathbf{r}) \times \mathbf{B} \rho dV \quad (8)$$

$$= \mathbf{E} \int_B \rho dV - (\mathbf{B} \times \mathbf{v}_o) \int_B \rho dV - \mathbf{B} \times \left(\boldsymbol{\omega}_{\mathcal{B}/\mathcal{E}} \times \int_B \mathbf{r} \rho \right) dV \quad (9)$$

$$= \mathbf{E} Q - (\mathbf{B} \times \mathbf{v}_o) Q - \mathbf{B} \times (\boldsymbol{\omega}_{\mathcal{B}/\mathcal{E}} \times \mathbf{q}_{\text{sep}}) \quad (10)$$

Where we have identified the total charge Q and defined the charge separation vector \mathbf{q}_{sep} as a generalization of the dipole moment.²³

$$Q = \int \rho dV \quad \text{and} \quad \mathbf{q}_{\text{sep}} = \int \mathbf{r} \rho dV \quad (11)$$

In many scenarios the orbital velocity \mathbf{v}_o , even taken in the ECEF frame, will dwarf the transport velocity $\boldsymbol{\omega}_{\mathcal{B}/\mathcal{E}} \times \mathbf{r}$. For a spacecraft with $r = 1$ m, $\boldsymbol{\omega}_{\mathcal{B}/\mathcal{E}} = 1$ deg/sec, and an ECEF orbital velocity of 1 km/sec, the ratio of the transport velocity to the orbital velocity will be less than 10^{-5} . In many scenarios the transport term can be dropped leaving:

$$\mathbf{F} = (\mathbf{E} + \mathbf{v}_o \times \mathbf{B}) Q \quad (12)$$

If the Voltage V is known, Q can easily be obtained through $Q = C V$ where C is the self capacitance. In flat fields, knowing the capacitance and orbital velocity is equivalent to knowing the force on the spacecraft. In vacuum, self capacitance will not change, so this parameter can be calculated at high accuracy before integration rather than inverting a $N \times N$ matrix at every integration time step to find the charges and summing over them as would need to be done with MSM.

Torque Derivation: Substituting the transport velocity expression into Eq. (7) and carrying through a triple product expansion and one cancellation the torque is found to be:

$$\mathbf{L} = -(\mathbf{E} + \mathbf{v}_o \times \mathbf{B}) \times \mathbf{q}_{\text{sep}} + \omega_{\mathcal{B}/\mathcal{E}} \times \int_{\mathcal{B}} (\mathbf{B} \cdot \mathbf{r}) \mathbf{r} \rho dV \quad (13)$$

$$= -(\mathbf{E} + \mathbf{v}_o \times \mathbf{B}) \times \mathbf{q}_{\text{sep}} + B \omega_{\mathcal{B}/\mathcal{E}} \times \int_{\mathcal{B}} (r^2 \cos(\theta)) \hat{\mathbf{r}} \rho dV \quad (14)$$

Where θ is defined as the angle between \mathbf{r} and \mathbf{B} . Much like a pendulum experiences a torque that aligns an offset mass with a gravity field, the first term describes a torque that aligns the dipole moment \mathbf{q}_{sep} with $\mathbf{E} + \mathbf{v}_o \times \mathbf{B}$. The second term provides a torque perpendicular to both the rotation and the magnetic field, and quadratically proportional to the charge separation. This term will only be significant when \mathbf{v}_o is comparable to $r\omega_{\mathcal{B}/\mathcal{E}}$, which will only happen in certain GEO orbits. If we neglect this term, the torque is given by:

$$\mathbf{L} = -(\mathbf{E} + \mathbf{v}_o \times \mathbf{B}) \times \mathbf{q}_{\text{sep}} \quad (15)$$

For the purposes of calculating torque, the full charge distribution in all nearly all orbits is captured by the electric dipole moment \mathbf{q}_{sep} . This also shows that there are limits on the torque that can be exerted on a passive space object. For instance in the absence of a significant magnetic field a torque cannot be produced parallel to either the \mathbf{E} field or the electric dipole moment \mathbf{q}_{sep} . For a spherical object, the dipole moment will be either parallel or anti-parallel to the electric field and no torque can be exerted. The relationship between the external electric field and the dipole is key to predicting de-spin effort.

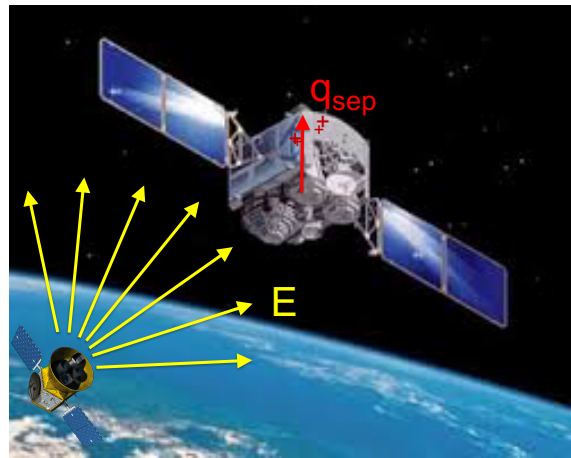


Figure 4. Radial E Field Configuration

Radial Electric Field Approximation

In some situations, one spacecraft can be approximated by a point and the other as a body as shown in Figure 4. The field at the body points radially away from the point charge and decreases as $1/r^2$.

Force Derivation: In a radial field, we can insert the point charge formula²³ for \mathbf{E} into Eq. (6):

$$\mathbf{E} = \frac{Q_1}{4\pi\epsilon_0 R^3} \mathbf{R} \quad (16)$$

$$\mathbf{F} = \frac{Q_1}{4\pi\epsilon_0} \int_B \frac{\rho}{R^3} \mathbf{R} dV \quad (17)$$

Here Q_1 is the point charge magnitude, \mathbf{R} points from the point charge to the volume element of the body, and \mathbf{r} points from the center of mass of the body to the volume element so $\mathbf{R} = \mathbf{R}_c + \mathbf{r}$ where \mathbf{R}_c points from the point charge to the center of mass of the body. If $R_c > r$, the denominator is expanded as:

$$R^{-3} = \frac{1}{R_c^3} \left(1 - \frac{3\mathbf{R}_c \cdot \mathbf{r}}{R_c^2} - \frac{3\mathbf{r} \cdot \mathbf{r}}{2R_c^2} + \frac{15}{2} \left(\frac{\mathbf{R}_c \cdot \mathbf{r}}{R_c^2} \right)^2 + \dots \right) \quad (18)$$

If this expression is inserted into Eq. (17), and terms 2nd order or higher in (r/R_c) are kept, the following force equation is obtained:

$$\begin{aligned} \mathbf{F} = \frac{Q_1}{4\pi\epsilon_0 R_c^3} & \left(\mathbf{R}_c \int_B \rho dV + \int_B \mathbf{r} \rho dV - \frac{3}{R_c^2} \int_B (\mathbf{r} \cdot \mathbf{R}_c) \mathbf{r} \rho dV - \frac{3}{R_c^2} \int_B (\mathbf{r} \cdot \mathbf{R}_c) \mathbf{R}_c \rho dV \right. \\ & \left. - \frac{3}{2R_c^2} \int_B (\mathbf{r} \cdot \mathbf{r}) \mathbf{R}_c \rho dV + \frac{15}{2R_c^4} \int_B (\mathbf{r} \cdot \mathbf{R}_c)^2 \mathbf{R}_c \rho dV \right) \end{aligned} \quad (19)$$

The first integral is the charge on the body Q_2 , which recovers the familiar expression

$$\mathbf{F} = \frac{Q_1 Q_2}{4\pi\epsilon_0 R^3} \mathbf{R} \quad (20)$$

The second integral is \mathbf{q}_{sep} . The vector property $(\mathbf{a} \cdot \mathbf{b})\mathbf{a} = ([\tilde{\mathbf{a}}][\tilde{\mathbf{a}}] + a^2[\mathbb{I}])\mathbf{b}$ is used to expand this equation. Where $[\tilde{\mathbf{r}}]$ is the matrix operation equivalent of the vector cross product $[\tilde{\mathbf{r}}] = \mathbf{r} \times$ and $[\mathbb{I}]$ is the identity matrix of appropriate size.

$$\begin{aligned} \mathbf{F} = \frac{Q_1}{4\pi\epsilon_0 R_c^3} & \left[Q_2 \mathbf{R}_c + \mathbf{q}_{\text{sep}} - \frac{3}{R_c^2} \left(\int_B ([\tilde{\mathbf{r}}][\tilde{\mathbf{r}}] + r^2[\mathbb{I}]) \rho dV \right) \mathbf{R}_c - \frac{3}{R_c^2} ([\tilde{\mathbf{R}}_c][\tilde{\mathbf{R}}_c] + R_c^2[\mathbb{I}]) \int_B \mathbf{r} \rho dV \right. \\ & \left. - \frac{3\mathbf{R}_c}{2R_c^2} \int_B r^2 \rho dV + \frac{15}{2R_c^4} \int_B (\mathbf{r} \cdot \mathbf{R}_c)^2 \mathbf{R}_c \rho dV \right] \end{aligned} \quad (21)$$

The second integral is \mathbf{q}_{sep} , and the last integral can be expanded as $(\mathbf{R}_c^T \mathbf{r} \mathbf{R}_c^T \mathbf{r}) \mathbf{R}_c = (\mathbf{R}_c \cdot ([\tilde{\mathbf{r}}][\tilde{\mathbf{r}}] + r^2[\mathbb{I}]) \mathbf{R}_c) \mathbf{R}_c$ and the earlier identity can be used in reverse order to yield:

$$\begin{aligned} \mathbf{F} = \frac{Q_1}{4\pi\epsilon_0 R_c^3} & \left[Q_2 \mathbf{R}_c + \mathbf{q}_{\text{sep}} - \frac{3}{R_c^2} (\mathbf{q}_{\text{sep}} \cdot \mathbf{R}_c) \mathbf{R}_c - \frac{3}{R_c^2} \left(\int_B ([\tilde{\mathbf{r}}][\tilde{\mathbf{r}}] + \frac{3}{2} r^2[\mathbb{I}]) \rho dV \right) \mathbf{R}_c \right. \\ & \left. + \frac{15}{2R_c^4} (\mathbf{R}_c \cdot \int_B ([\tilde{\mathbf{r}}][\tilde{\mathbf{r}}] + r^2[\mathbb{I}]) \mathbf{R}_c \rho dV) \mathbf{R}_c \right] \end{aligned} \quad (22)$$

The inertia tensor is defined as $\int_B -[\tilde{\mathbf{r}}][\tilde{\mathbf{r}}] dm$,²⁴ where $[\tilde{\mathbf{r}}] = \mathbf{r} \times$ is the matrix operation equivalent of the vector cross product. If we make a similar definition for the charge tensor our analysis greatly simplifies.

$$[Q] = \int_B -[\tilde{\mathbf{r}}][\tilde{\mathbf{r}}] \rho dV \quad (23)$$

We also note that $\int_B r^2 \rho dV$ is half the trace of the charge tensor.

$$\mathbf{F} = \frac{Q_1}{4\pi\epsilon_0 R_c^3} \left[Q_2 \mathbf{R}_c + \mathbf{q}_{\text{sep}} - \frac{3}{R_c^2} (\mathbf{q}_{\text{sep}} \cdot \mathbf{R}_c) \mathbf{R}_c + \frac{3}{R_c^2} \left([Q] - \frac{3}{4} \text{trace}([Q]) \right) \mathbf{R}_c \right. \\ \left. + \frac{15}{2R_c^4} (\mathbf{R}_c \cdot [Q] \mathbf{R}_c + \frac{R_c^2}{2} \text{trace}([Q]) \mathbf{R}_c \right] \quad (24)$$

Which can be simplified to give our final result

$$\mathbf{F} = \frac{Q_1}{4\pi\epsilon_0 R_c^3} \left[Q_2 \mathbf{R}_c + \mathbf{q}_{\text{sep}} - \frac{3(\mathbf{q}_{\text{sep}} \cdot \mathbf{R}_c)}{R_c^2} \mathbf{R}_c + \frac{3[Q] \mathbf{R}_c}{R_c^2} - \frac{3\mathbf{R}_c \text{trace}([Q])}{2} \right. \\ \left. + \frac{15}{2R_c^2} (\hat{\mathbf{e}}_r \cdot [Q] \hat{\mathbf{e}}_r) \mathbf{R}_c \right] \quad (25)$$

Where $\hat{\mathbf{e}}_r$ is a unit vector in the direction of \mathbf{R}_c . There are many striking things about this equation; there are three terms in the radial (\mathbf{R}_c) direction, and three in non-radial directions, a very unintuitive but interesting result.

If we define r_s as the craft radius, the upper bound for the magnitude of \mathbf{q}_{sep} is $r_s Q$, and the upper bound the elements of $[Q]$ is $Q r_s^2$. Since in all but docking cases $R_c > r_s$, the relative magnitudes of the terms in the upper expression can be compared. The only zeroth-order term in r_s/R_c is the first one: Q_2 . The fourth and sixth terms are first order, and the rest are second order. The zeroth order term depends on Q , the first order terms depend on \mathbf{q}_{sep} , and the second order terms depend on $[Q]$. This force expression is very similar to the way forces in an inverse-square gravity field are expressed, only allowing for an origin not-aligned with the center of mass and using the charge tensor rather than the inertia tensor. If the center of mass was aligned with the center of charge, \mathbf{q}_{sep} would always be zero. If the second order terms are dropped the force expression becomes:

$$\mathbf{F} = \frac{Q_1 Q_2}{4\pi\epsilon_0 R_c^3} \left(\mathbf{R}_c - \frac{3(\mathbf{R}_c \cdot \mathbf{q}_{\text{sep}})}{R_c^2 Q_2} \mathbf{R}_c + \frac{\mathbf{q}_{\text{sep}}}{Q_2} \right) \quad (26)$$

We are left with two non-standard terms, the magnitude of each depends on q_{sep}/Q_2 , but only one depends on \mathbf{q}_{sep} for direction. The third term gives a force dependent on the dipole moment solely for direction. For a many objects, the dipole moment will be greatest along the direction of \mathbf{E} , so these terms would not change the direction of the force. Once again the connection between the dipole moment and the external field (which has direction \mathbf{R}_c in this case) is key to understanding this non-intuitive behavior.

Torque Derivation: Inserting the point charge expression for \mathbf{E} into the torque equation in Eq. (7) gives:

$$\mathbf{L} = \int_B \mathbf{r} \times \frac{Q}{4\pi\epsilon_0 R^3} \mathbf{R} \rho dV \quad (27)$$

We can use the same expansion for R^{-3} as before to get:

$$\mathbf{L} = -\frac{Q_1}{4\pi\epsilon_0} \mathbf{R}_c \times \int_B \mathbf{r} \frac{1}{R_c^3} \left(1 - \frac{3\mathbf{R}_c \cdot \mathbf{r}}{R_c^2} - \frac{3\mathbf{r} \cdot \mathbf{r}}{2R_c^2} + \frac{15}{2} \left(\frac{\mathbf{R}_c \cdot \mathbf{r}}{R_c^2} \right)^2 \right) \rho dV \quad (28)$$

This can be expanded using vector identities to give:

$$\mathbf{L} = -\frac{Q_1}{4\pi\epsilon_0 R_c^3} \mathbf{R}_c \times \left[\int_B \mathbf{r} \rho dV - \frac{3}{R_c^2} \int_B ((\mathbf{r} \times \mathbf{r}) \times \mathbf{R}_c - (\mathbf{r} \cdot \mathbf{r}) \mathbf{R}_c) \rho dV \right. \\ \left. - \frac{3}{2R_c^2} \int_B r^2 \mathbf{r} \rho dV + \frac{15}{2R_c^2} \int_B \mathbf{R}_c \cdot [\mathbf{r} \times (\mathbf{r} \times \mathbf{R}_c) + r^2 \mathbf{R}_c] \rho dV \mathbf{R}_c \right] \quad (29)$$

$$= -\frac{Q_1}{4\pi\epsilon_0 R_c^3} \mathbf{R}_c \times \left[\mathbf{q}_{\text{sep}} + \frac{3}{R_c^2} [Q] \mathbf{R}_c - \frac{3}{2R_c^2} \int_B r^2 \mathbf{r} \rho dV \right] \quad (30)$$

There are no zeroth-order terms in this expression. If we use the same magnitude bounds as were used in the Radial Force section and keep only the 1st and 2nd order terms in r/R_c we are left with:

$$\mathbf{L} = \frac{Q_1}{4\pi\epsilon_0 R_c^3} \left[\mathbf{q}_{\text{sep}} + \frac{3}{R_c^2} [Q] \mathbf{R}_c \right] \times \mathbf{R}_c \quad (31)$$

If the charge tensor $[Q]$ is small, or even if it is large but diagonal with similarly sized entries the second term will not contribute. If we further simplify and only keep the first order term we are left with

$$\mathbf{L} = \frac{Q_1}{4\pi\epsilon_0 R_c^3} \mathbf{q}_{\text{sep}} \times \mathbf{R}_c \quad (32)$$

This describes a torque which acts to align the \mathbf{q}_{sep} with the direction of \mathbf{E} at the center of the body. Once again, the dipole moment drives the system. In a perfectly symmetric object such as a sphere, the dipole will be either parallel or antiparallel to the field, (which is in the \mathbf{R}_c direction in this case). This means that no torque can be produced. More generally, the geometry of the passive body must allow \mathbf{q}_{sep} to grow in a direction perpendicular to the source of the point field. To apply this to our cylinder example, the torque must be zero in the 0° and 90° cases and the torque would be larger at non-zero angles if the cylinder was longer.

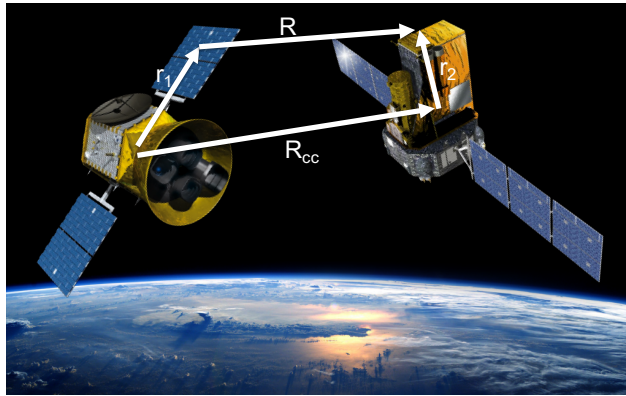


Figure 5. Coordinate set for general body formulation.

General Bodies:

For two general bodies we can assume nothing about the form of the field between them. The force and torque on body 2 subject to an arbitrary charge distribution on body 1 is given by:

$$\mathbf{F}_2 = \frac{1}{4\pi\epsilon_0} \int_{B_2} \left(\int_{B_1} \frac{\mathbf{R}_{cc} + \mathbf{r}_2 - \mathbf{r}_1}{(R_{cc} + r_2 - r_1)^3} \rho_1 dV_1 \right) \rho_2 dV_2 \quad (33)$$

$$\mathbf{L}_2 = \frac{1}{4\pi\epsilon_0} \int_{B_2} \mathbf{r}_2 \times \left(\int_{B_1} \frac{\mathbf{R}_{cc} - \mathbf{r}_1}{(R_{cc} + r_2 - r_1)^3} \rho_1 dV_1 \right) \rho_2 dV_2 \quad (34)$$

Where \mathbf{R}_{cc} points from center of mass of body 1 to the center of mass of body 2, and \mathbf{r}_1 and \mathbf{r}_2 point to the volume elements of body 1 and 2, respectively, as shown in Figure 5. These integrals are intractable, and must be approximated. The force between two charges q_1 and q_2 is given by

$$\mathbf{F}_c = \frac{q_1 q_2}{4\pi\epsilon_0 r^3} \mathbf{r} \quad (35)$$

Where \mathbf{r} points from one charge to another. This formula can be used in place of the differential force given by Eq. (5) and applied to the MSM force and torque Eq. (3) and (4) to yield:

$$\mathbf{F}_2 = \sum_{i=1}^m \sum_{j=1}^n \frac{q_i q_j}{R_{i,j}^3} \mathbf{R}_{i,j} \quad (36)$$

$$\mathbf{L}_2 = \sum_{i=1}^m \sum_{j=1}^n \mathbf{r}_2 \times \left(\frac{q_i q_j}{R_{i,j}^3} \mathbf{R}_{i,j} \right) \quad (37)$$

Where the charge distribution on body 1 and 2 are approximated into m and n spheres in an MSM model. This recovers the standard MSM formulation.^{21,22}

AFM VALIDATION

While AFMs are an elegant and first-principles approach to predicting the force and torque on a spacecraft subjected to an external field, numerous expansions were truncated to arrive at the results. To test them we use the results produced using the commercial FEA software package ANSYS Maxwell as a truth model and compare the force and torque predicted using AFMs against it. Maxwell was used in many runs, and for each the total charge, dipole moment, force, and torque were recorded as well as the external fields.

Flat Fields

To create a locally flat electric field, two large (60m x 60m x 0.6m) plates are separated by 18 meters along the y axis and a cylinder (diameter = 1m, length = 3m) is placed in between them.

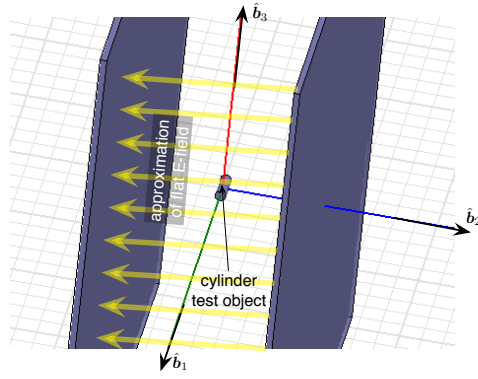
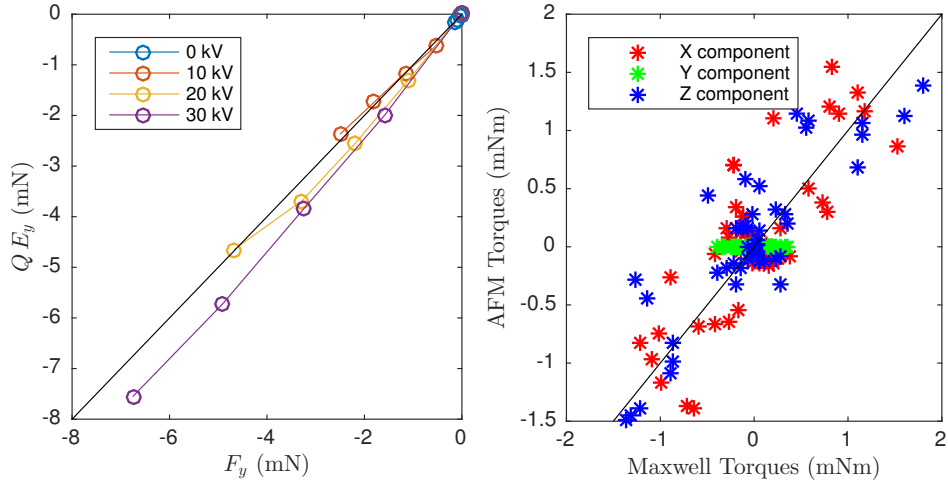


Figure 6. Maxwell setup for flat fields case. The plates are charged oppositely to create a strong electric field in the y direction.

Force Validation: The plates are subjected to a charge density varying from 0 to $\pm 40 \text{ nC/m}^3$, creating an electric field ranging from 0 to 2.71 kV/m. The cylinder was also independently charged to 0, 10, 20 and 30 kV. The charged cylinder feels a force in this strong electric field which is recorded and compared to the force predicted using Eq. (12)



(a) Comparison of predicted AFM force to measured Maxwell force (b) Comparison of predicted AFM torque to measured Maxwell force

Figure 7. AFM force and torque prediction in a flat field.

The force predicted by AFMs is close to the truth model, and this agreement is best at low cylinder voltages. If we define the percent error as

$$\text{Percent Error} = 100 \frac{\sum |F_{\text{AFM}} - F_{\text{Max}}|}{\sum |F_{\text{Max}}|} \quad (38)$$

the percent error is 11.6%.

Torque Validation: The same two plates are used again, but rather than sweeping across cylinder voltage and charge density on the plates, the plates are held at $\pm 80 \text{ nC/m}^3$ and the cylinder is held at

30 kV and 3-2-1 Euler angles are used to rotate the cylinder through pitch and yaw since a roll would only rotate the cylinder about its long axis and wouldn't give new results. The dipole is recorded in Maxwell and is used along with the known E field to predict an AFM torque using Eq. (15).

The torque errors are much larger in this formulation. Each component of the torque is compared in the figure above with red, green, and blue asterisks showing the x,y, and z components respectively. Both plates are perpendicular to the y-axis, which means that the E field ought to be parallel to the y-axis. If the E field is parallel to the y-axis then there should be no torque about that axis following Eq. (15). The AFM torque predicts this, but the y component of the measured Maxwell torque is non-zero. This indicates that using two charged plates does not create a perfectly flat field. To quantify this, the percent error can be computed for each axis, and yields values of 80.9%, 100% and 56.6% for the x,y, and z components. Eq. (38) was used once again to compute the error.

Radial Fields

To make a radial field in Maxwell, a small sphere containing a large charge ($30 \mu\text{Coulomb}$) was placed at each point in the Figure 8(a) while the cylinder was held at 30 kV. The sample grid is the set of points from 5 to 10 meters away from the center of the cylinder, and every 15° from 0° to 90° . The force and torque were predicted using Eqns. (26) and (32).

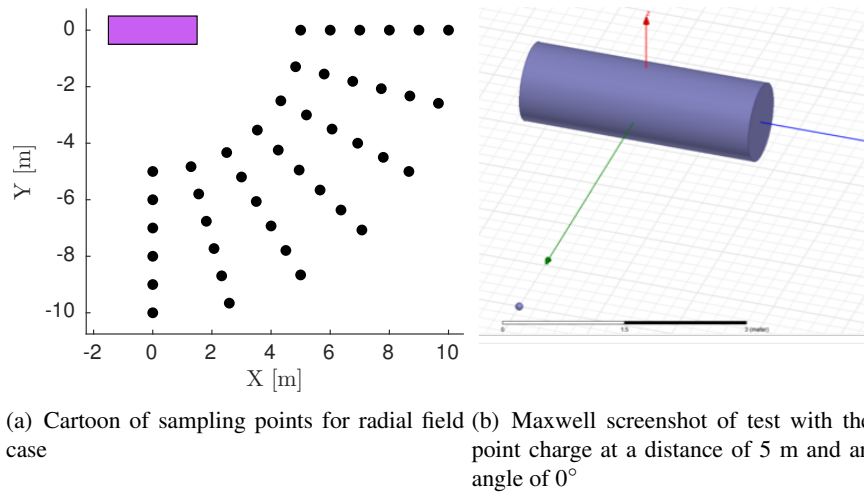
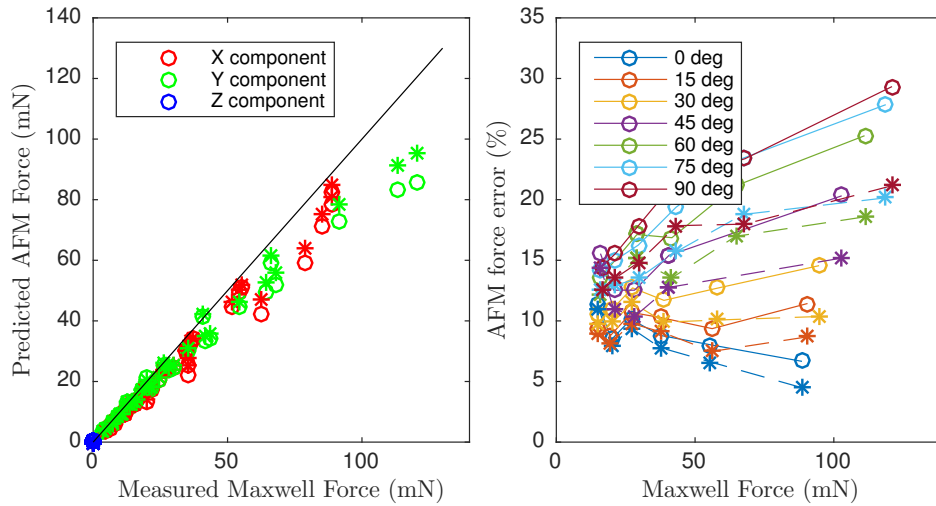


Figure 8. Schematic showing the test setup for radial fields. The cylinder is charged to 30 kV and the point is charged with $30 \mu\text{Coulombs}$.

Force Validation: For a radial field, we can use either a zeroth, first, or second order force expression. The zeroth order expression recovers the standard Coulomb expression, the first order expression has some information about the alignment of the dipole and the central direction, and the second order expression depends on the charge tensor. A plot of the force predicted by AFMs in both a zeroth and a first order expansion is given below. The dashed lines and asterisks indicate the first order expansion while the straight lines and circles indicate the zeroth order expansion.



(a) Comparison of predicted AFM force to measured Maxwell force (b) Force percent errors for the radial force case

Figure 9. Zeroth and first order force percent errors predicted using AFMs are plotted against measured forces in ANSYS Maxwell. Dashed lines indicate first order solutions while straight lines indicate zeroth order solutions

The forces predicted using AFMs are consistently lower than the Maxwell truth model, especially in the near field. The error percent of the norm of the vector difference is also plotted in Figure 9(b). The first order correction always lowers the error, but never much below 5°. The correction is more dramatic when the zeroth order error is large. The error is also nearly always larger at high angles, corresponding to the sphere being close to the long axis of the cylinder. This is somewhat intuitive, as induced effects will be most significant in this situation.

Torque Validation: There is no zeroth order term for torque. The first order term is given by Eq. (32). This equation is evaluated at all data points except for the 0° and 90° cases which should produce no torque. The results are plotted in Figure 10. AFMs consistently under predict the torque by a factor of roughly 5. The reason for this discrepancy is still being investigated.

PREDICTION OF CHARGE DISTRIBUTION DYNAMICS

The force and torque depend on the external fields as well as the charge distribution within the body as shown in Eqns. (6) and (7). This charge distribution can be approximated by using the dipole moment \mathbf{q}_{sep} and the charge tensor $[Q]$. While this formulation is elegant and simple, it relies on knowledge of the charge distribution, which isn't known a priori. Additionally, how the charge distribution changes due to external fields is of vital importance for high fidelity orbit propagation. The state \mathbf{q}_{sep} is the dominant term in the torque equation, and the first-order correction for force. If a locally flat field is assumed, \mathbf{q}_{sep} can be predicted without resorting to commercial FEA software allowing for fast computation.

Because \mathbf{q}_{sep} was defined relative to the center of mass, it will have some intrinsic value due to the geometry of the conducting body. Consider a satellite with a long slender boom—while the center of mass will be near the bus, the center of charge could easily be in the center of the boom, many meters from the center of mass. This will cause a non-zero value for \mathbf{q}_{sep} even in the absence of

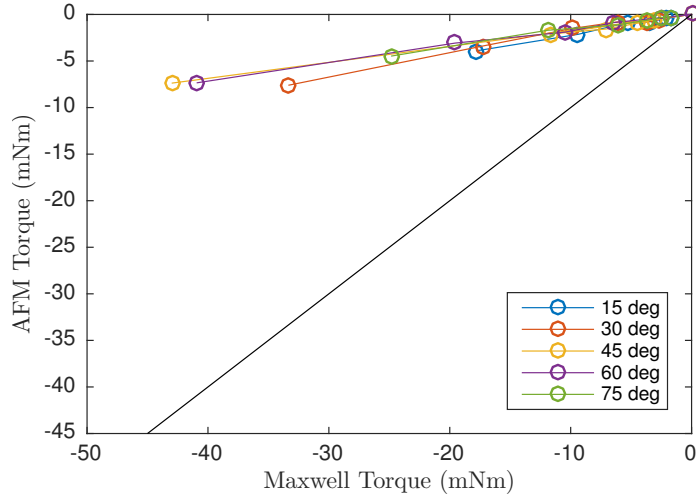


Figure 10. Comparison of AFM predicted torque with Maxwell generated torque, the black line has slope equal to one.

external fields. This geometric $\mathbf{q}_{\text{sep}_g}$ will increase with Voltage and can be calculated either in a commercial FEA software package by finding the slope of a plot of \mathbf{q}_{sep} . If an external electric field is present, the electrons in the spacecraft will move opposite the direction of the field which will create an induced dipole moment parallel to the field. The susceptibility of the dipole moment to a constant external field will be derived in an MSM formulation.

The Voltage difference between two points separated by \mathbf{r} in a flat \mathbf{E} field is given by:

$$\Delta V = - \int_1^2 \mathbf{E} \cdot d\mathbf{r} = -\mathbf{E} \cdot \mathbf{r}_{1,2} \quad (39)$$

Voltage is a linear field, so the total Voltage of each sphere is that due to the charge on nearby spheres, and that due to the external field:

$$\mathbf{V} = [C]^{-1}\mathbf{q} - [R]\mathbf{E} \quad (40)$$

Where $[R]$ is a matrix of the positions of each sphere in the MSM model measured from the center of mass.

$$[R] = \begin{bmatrix} r_x & r_y & r_z \\ \vdots & \vdots & \vdots \end{bmatrix} \quad (41)$$

Inverting the equation for the charge on each sphere yields

$$\mathbf{q} = [C](\mathbf{V} + [R]\mathbf{E}) \quad (42)$$

\mathbf{q}_{sep} can now be easily formed.

$$\mathbf{q}_{\text{sep}} = [R]^T \mathbf{q} \quad (43)$$

$$= [R]^T [C](\mathbf{V} + [R]\mathbf{E}) \quad (44)$$

$$= ([R]^T [C])\mathbf{V} + ([R]^T [C][R])\mathbf{E} \quad (45)$$

Since we are considering a conducting body, every element of \mathbf{V} is the common surface potential V , so we can pull out the scalar Voltage V and the external field \mathbf{E} and define the coefficients as the geometric dipole moment and the susceptibility matrix.

$$\mathbf{q}_{\text{sep}} = \mathbf{q}_g V + [\chi] \mathbf{E} \quad (46)$$

Where these new parameters are defined in a MSM formulation as

$$\mathbf{q}_g = [R]^T [C] \text{ones}(N,1) \quad \text{and} \quad [\chi] = [R]^T [C] [R] \quad (47)$$

The geometric dipole moment describes the intrinsic dipole moment that is produced by the center of mass and center of charge not necessarily being aligned, and the susceptibility matrix describes the first-order sensitivity of the dipole moment to an external electric field. This equation can be used to predict the electric dipole moment of a spacecraft in a changing locally-flat electric field, which allows us to compute the changing electrostatic force and torque on a spacecraft.

Linear Least-Squares Determination of Susceptibility Matrix

Because the new parameters are defined in terms of body-fixed quantities ($[R]$ and $[C]$) the parameters \mathbf{q}_g and $[\chi]$ are constant and fixed in the body frame. To find them, we apply an electric field in different body-directions while the cylinder is charged to different levels using Maxwell. The method that was described in the flat torque section is used, holding two plates at opposite charges and the cylinder at a high voltage while rotating it through pitch and yaw in steps of 30° from 0° to 180° .

The vector \mathbf{q}_g describes the offset of the center of mass from the center of charge, which for our test cylinder should be zero because we have defined the center of mass to be at the geometric center of the cylinder. The matrix $[\chi]$ describes the ability of an electric field to create a dipole moment. The diagonal elements of $[\chi]$ describe the ability of a parallel field to move charge along one of the cylinder's principal axis. The diagonal element that corresponds to the long axis of the cylinder ((1,1) for in this coordinate system) should be much larger than the other two, which should be roughly equal. The off-diagonal terms should be zero since we have picked what ought to be a principal frame, and any non-zero values probably correspond to noise in the FEA solution.

To create the susceptibility matrix, we let the geometric dipole be zero and use only the first 3 values for pitch and yaw. We then re-form Eqn (46) as:

$$\begin{bmatrix} \mathbf{q}_{\text{sep}_x} & \dots \\ \mathbf{q}_{\text{sep}_y} & \dots \\ \mathbf{q}_{\text{sep}_z} & \dots \end{bmatrix} = [\chi] \begin{bmatrix} E_x & \dots \\ E_y & \dots \\ E_z & \dots \end{bmatrix} \quad (48)$$

The linear least squares solution to this overdetermined system is found using Matlab's backslash operator, and gives a numerical value for $[\chi]$ of:

$$[\chi] = 10^{-9} \begin{bmatrix} 0.1285 & -0.0028 & -0.0066 \\ -0.0004 & 0.0299 & 0.0023 \\ 0.0004 & -0.0013 & 0.0299 \end{bmatrix} \text{ F m}^2 \quad (49)$$

As predicted, the (1,1) element is the largest, the (2,2) and (3,3) elements are smaller and identical up to the fourth significant figure, and the rest of the elements are smaller still and correspond to noise.

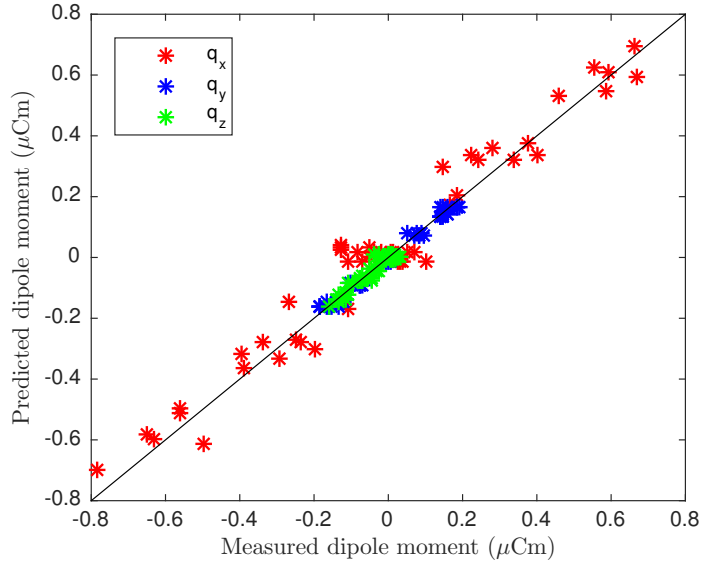


Figure 11. Prediction of dipole moment using AFMs. Red, Blue, and Green points correspond to x,y, and z components of the dipole moment

Validation of Charge Distribution Dynamics

The susceptibility matrix was found using only the first 3 of the 7 sampled points for pitch and yaw. This matrix will now be used to predict the dipole moment for the entire set of data using Eq. (46) with the geometric dipole set to zero and the $[\chi]$ shown above. The prediction is accurate and has a percent error of only 4.21% if we re-purpose Eq. (38).

CONTROLLABILITY

If the geometric dipole is zero, the susceptibility matrix is the main driver in how the dipole moment responds to an external electric field. In a flat field the torque will be given by:

$$\mathbf{L} = \mathbf{q}_{\text{sep}} \times \mathbf{E} \quad (50)$$

$$= (\mathbf{q}_g V + [\chi] \mathbf{E}) \times \mathbf{E} \quad (51)$$

$$= -[\tilde{\mathbf{E}}] \mathbf{q}_g V - [\tilde{\mathbf{E}}][\chi] \mathbf{E} \quad (52)$$

The torque is amplified by a strong \mathbf{E} field as well as a high voltage, which matched intuition. Objects with either large geometric dipoles, corresponding to cases where the center of mass and center of charge are far apart, or large susceptibilities will also feel stronger torques. If the geometric dipole is zero, as it is for our cylinder example, the torque equation reduces to a rather elegant result.

$$\mathbf{L} = -[\tilde{\mathbf{E}}][\chi] \mathbf{E} \quad (53)$$

If the diagonal elements of $[\chi]$ are all identical, the dipole moment will be parallel to the external field and no torque can be exerted. If two are identical, as with the cylinder, there is one body axis about which torques cannot be exerted. If no two diagonal elements are the same, then general 3D torques can be exerted. The effort needed to produce these torques is a function of how close to perpendicular the dipole is to the external field. A rough proxy of this effort is the ratio of each diagonal element of $[\chi]$ to the smallest diagonal element of $[\chi]$.

Euler's equation in the case of no geometric dipole can be written in the following elegant form:

$$[I]\dot{\omega} = [\tilde{\omega}][I]\omega - [\tilde{E}][\chi]E \quad (54)$$

The susceptibility matrix is of comparable importance to the inertia matrix for the purpose of changing the body rates (ω) using electrostatic torques. If the geometric dipole is non-zero, more detailed analysis must be taken.

CONCLUSION

Appropriate Fidelity Measures (AFMs) are derived from first-principles to predict the force and torque on a spacecraft in flat and radial fields. The predicted force deviated from the truth model by 11.6% for force and 56-100% for torque in the flat fields case. For the radial fields case the force error was 16.9% for the first order solution, and 13.4% for the second order solution. The predicted torque is less than the truth model by roughly a factor of 5. Some of this discrepancy may be due to implementation issues in Maxwell. All of these results are outperformed by pre-existing MSM models for force and torque prediction which consistently achieve less than 1% error. The dynamics of the charge distribution as described with these AFMs are derived in an MSM formulation and show good agreement (4.2% error) with the measured data. Added insight to the problem of controllability while de-spinning is gained through the analytical structure of the analytical expansions.

ACKNOWLEDGEMENT

The authors would like to thank Philip Chow for his assistance with the FEA truth model. This work was funded by research grant No. FA9550-15-1-0407 from the Air Force Office of Space Research.

REFERENCES

- [1] J. F. Fennell, H. C. Koons, M. Leung, and P. Mizera, "A review of SCATHA satellite results: Charging and discharging," *1983.*, 1983, pp. 3–11.
- [2] C. Früh, D. Ferguson, C. Lin, and M. Jah, "The Effect of Passive Electrostatic Charging on Near-Geosynchronous High Area-To-Mass Ratio Objects," *International Astronautical Congress*, Vol. 64, 2013.
- [3] D. A. Vallado, *Fundamentals of Astrodynamics and Applications*. Microcosm Press, 4th ed., March 2013.
- [4] H. Schaub and L. E. Z. Jasper, "Orbit Boosting Maneuvers for Two-Craft Coulomb Formations," *AIAA Journal of Guidance, Control, and Dynamics*, Vol. 36, Jan. – Feb. 2013, pp. 74–82.
- [5] D. F. Moorer and H. Schaub, "Electrostatic Spacecraft Reorbiter," US Patent 8,205,838 B2, Feb. 17 2011.
- [6] K. K. Galabova, *Architecting a Family of Space Tugs Based on Orbit Transfer Mission Scenarios*. PhD thesis, Massachusetts Institute of Technology, Cambridge, MA, Feb. 2004.
- [7] H. Schaub and D. F. Moorer, "Geosynchronous Large Debris Reorbiter: Challenges and Prospects," *The Journal of the Astronautical Sciences*, Vol. 59, No. 1–2, 2014, pp. 161–176.
- [8] H. Schaub and Z. Sternovsky, "Active Space Debris Charging for Contactless Electrostatic Disposal Maneuvers," *6th European Conference on Space Debris*, Darmstadt, Germany, ESOC, April 22–25 2013. Paper No. 6b.O-5.
- [9] P. V. Anderson and H. Schaub, "Local Debris Congestion in the Geosynchronous Environment With Population Augmentation," *6th European Conference on Space Debris*, Darmstadt, Germany, ESOC, April 22–25 2013. Paper No. 3a.P-3.
- [10] P. V. Anderson and H. Schaub, "Local Orbital Debris Flux Study in the Geostationary Ring," *Advances in Space Research*, Vol. 51, No. 12, 2013, pp. 2195–2206, 10.1016/j.asr.2013.01.019.

- [11] T. Bennett, D. Stevenson, E. Hogan, L. McManus, and H. Schaub, "Prospects and Challenges of Touchless Debris Despinning Using Electrostatics," *3rd European Workshop on Space Debris Modeling and Remediation*, CNES, Paris, June 16–18 2014.
- [12] T. Bennett and H. Schaub, "Touchless Electrostatic Three-Dimensional Detumbling of Large GEO Debris," *AAS/AIAA Spaceflight Mechanics Meeting*, Jan. 26–30 2014.
- [13] E. Hogan and H. Schaub, "Collinear Invariant Shapes for Three-Craft Coulomb Formations," *Acta Astronautica*, Vol. 12, March–April 2012, pp. 78–89, 10.1016/j.actaastro.2011.10.020.
- [14] H. Vasavada and H. Schaub, "Analytic Solutions for Equal Mass Four-Craft Static Coulomb Formation," *Journal of the Astronautical Sciences*, Vol. 56, Jan. – March 2008, pp. 17–40.
- [15] J.-H. Chong, "Dynamic Behavior of Spacecraft Formation Flying using Coulomb Forces," Master's thesis, Michigan Technological University, May 2002.
- [16] P. Janhunen, "Electrostatic Sail for Producing Spacecraft Propulsion," US Patent 2007099201, Feb 2006.
- [17] M. A. Peck, "Prospects and Challenges for Lorentz-Augmented Orbits," *AIAA Guidance, Navigation and Control Conference*, San Francisco, CA, August 15–18 2005. Paper No. AIAA 2005-5995.
- [18] B. Streetman and M. A. Peck, "New Synchronous Orbits Using the Geomagnetic Lorentz Force," *AIAA Journal of Guidance, Control, and Dynamics*, Vol. 30, Nov.–Dec. 2007, pp. 1677–1690.
- [19] M. A. Peck, B. Streetman, C. M. Saaj, and V. Lappas, "Spacecraft Formation Flying using Lorentz Forces," *Journal of British Interplanetary Society*, Vol. 60, July 2007, pp. 263–267.
- [20] B. Streetmann and M. A. Peck, "Gravity-Assist Manuevers Augmented by the Lorentz Force," *Journal of Guidance, Control, and Dynamics*, Vol. 32, October 2009.
- [21] D. Stevenson and H. Schaub, "Multi-Sphere Method for Modeling Electrostatic Forces and Torques," *Advances in Space Research*, Vol. 51, Jan. 2013, pp. 10–20, 10.1016/j.asr.2012.08.014.
- [22] D. Stevenson and H. Schaub, "Multi Sphere Modeling for Electrostatic Forces on Three-Dimensional Spacecraft Shapes," *AAS/AIAA Spaceflight Mechanics Meeting*, Charleston, South Carolina, Jan. 29 – Feb. 2 2012.
- [23] D. J. Griffiths, *Introduction to Electrodynamics*. Prentice Hall, 3rd ed., 1999.
- [24] H. Schaub and J. L. Junkins, *Analytical Mechanics of Space Systems*. Reston, VA: AIAA Education Series, 2nd ed., October 2009.